J. Fluid Mech. (1987), vol. 185, pp. 483–502
Printed in Great Britain

Turbulence in radial flow between parallel disks at medium and low Reynolds numbers

By M. TABATABAI† AND A. POLLARD
Department of Mechanical Engineering, Queen's University, Kingston, Ontario, Canada, K7L 3N6

(Received 6 May 1986 and in revised form 12 March 1987)

The radial flow of air between two closely spaced parallel disks is studied experimentally and the behaviour of the flow, especially the turbulence decay mechanism, is examined. At high Reynolds numbers the flow resembles fully developed turbulent two-dimensional channel flow. A quasi-laminar boundary layer is found to gradually replace the viscous sublayer as the Reynolds number decreases. At low Reynolds numbers, the turbulence decays and the flow gradually approaches a laminar-type profile. The decay process is shown to be very slow and indications of a weak turbulence-generating mechanism is observed even at very low Reynolds numbers. Relaminarization, rather than being an abrupt change in the state of the flow, is an eventual outcome of the turbulence decay process.

1. Introduction

The radial flow of fluids between parallel plates or disks is of both academic and industrial interest. The academic interest stems from the continuous increase in the cross-sectional area of the flow which results in a gradual decrease in the Reynolds number. The flow can therefore be considered a special case of plane two-dimensional channel flow with the potential for relaminarization. The industrial interest is related to the flow in radial diffusers, non-rotating air bearings, disk-type heat exchangers and pneumatic micrometers.

The laminar radial flow between parallel disks has been studied by many investigators; for example, McGinn (1955), Livesey (1959), Savage (1964), Jackson & Symmons (1965), Ishizawa (1965, 1966), Moller (1963) and Mochizuki & Yang (1983, 1985), Mochizuki, Yang & Tanaka (1986). The major emphasis of these studies was to determine, or theoretically predict, the pressure recovery of the flow and to present a criterion for separation which occurs since the fluid normally must undergo a sharp 90° bend before it enters the space between the disks. These studies have produced theoretical expressions for the pressure recovery which are, except in the inlet region, in accord with the experimental values. Various empirical criteria for the Reynolds number below which separation does not occur have also been put forward (for example $Re_{r,R_1} = 11.0$ (Mochizuki & Yang 1983, 1985) where $Re_{r,R_1} = Re_m (2h/R_1)^2$ and Re_m is the Reynolds number based on the local mean velocity U and radius r, R_1 is the inlet radius and h is half the gap width between the disks).

Mochizuki and co-workers also have investigated, through flow visualization and laminar calculations using finite-volume techniques, the flow through parallel disks. They provide qualitative arguments about the evolution and the stability of the flow

† Now at: Ontario Hydro, Toronto.

as it expands from a condition of uniform inlet velocity profile at the entrance to the disks.

Moller (1963) used Pitot static tubes to obtain the first extensive measurements of the mean velocity characteristics for the case of turbulent flow. He suggested that, in radial flows, relaminarization occurs and is due to the thickening of the viscous sublayer. Peube, as reported by Kreith (1966), established analytically that the velocity profiles in laminar radial flows contain an inflexion point at radial distances less than a critical value r_c, obtained from

$$\frac{r_c}{h} = k\left(\frac{Q}{\nu h}\right), \tag{1}$$

where Q is the volume flow rate, and $k = 0.218$. Chen & Peube (1964) suggested the idea of a critical radius for the inception of reverse transition. Kreith (1966), too, argued that reverse transition cannot take place unless the flow condition permits the existence of a laminar velocity profile. He then suggested (1) with $k = 0.28$ as the criterion for the radius after which relaminarization is achieved. Later experiments by Bakke & Kreith (1969) concluded that relaminarization is only approached but never reached. The critical-Reynolds-number criteria for relaminarization, presented by Moller (1963) and Kreith (1966), were also invalidated by Bakke & Kreith. These latter authors reasoned that since the radial turbulence-energy production $(-\overline{u'^2}\mathrm{d}U/\mathrm{d}r)$ is negative, the turbulence energy increases in the radial direction; however, note that this turbulence-energy term, although positive, in most relevant cases is small when compared to the turbulence-dissipation term, and it can not be considered the sole turbulence-maintaining mechanism in radial flows.

Higgins (1975), using hot-wire anemometry, measured the turbulence-intensity variations in radial flow between parallel disks. Based on these measurements, he suggested a value of $Re_{r,r} = 8.0$ for the onset of the decay process (where $Re_{r,r} = Re_m (2h/r)$ is the reduced Reynolds number and $2h$ is the gap width). Higgins did not study the characteristics of this decay.

The purpose of the present contribution is to provide the first comprehensive study of the radial flow problem at low to medium Reynolds numbers. The apparatus design allowed for a fairly large local Reynolds number ($Re_{l,r} = 2Uh/\nu$) drop for each flow rate. First-, second-, third- and fourth-order moments of the fluctuating velocity, probability density and spectra are provided. Relevant comparisons are made with two-dimensional channel flows and a physical model for the decay process is suggested that incorporates the concepts of near-wall flow 'structures' as used in boundary layers (see, for example, Zaric 1975).

2. Experimental procedure

The apparatus used for the present study (figure 1) consisted of two 2.5 cm thick, accurately surface finished, aluminium plates, each 1.2 m in diameter ($2R_2$). The disks were held apart by means of six equally spaced, precisely machined spacer blocks providing a gap width $2h$ of 1.0 cm. The flow was provided by a 5 hp centrifugal fan and was passed through a bleeding valve, a settling box, a PVC pipe (containing honeycomb) and a settling chamber (containing a filter and an array of screens, and with a diametrical contraction ratio of 26:1). A shaped inlet and an inlet piece, designed according to the recommendations of Moller (1966), were used to direct the flow between the disks. On the upper disk, 21 pressure taps were placed

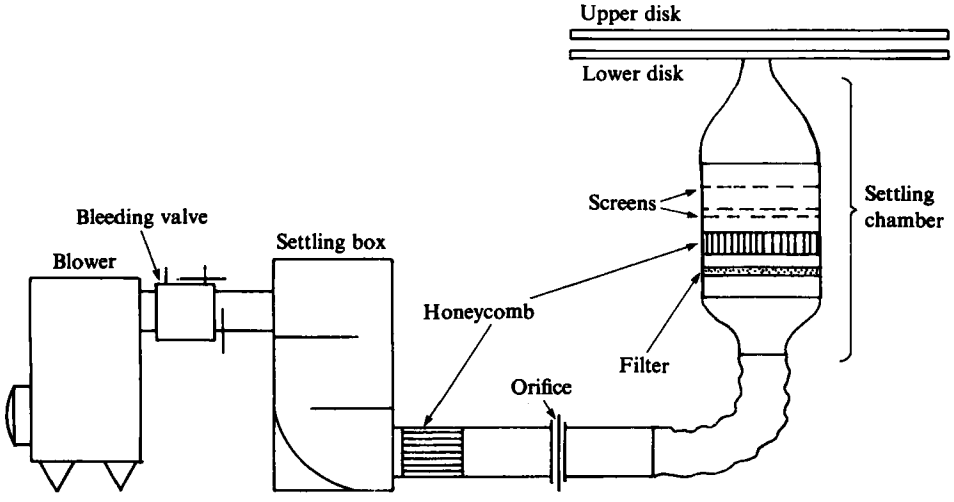

FIGURE 1. Schematic of the apparatus.

along the disk radius for measuring the static pressure distribution. Six additional pressure taps, drilled in a line normal to the main pressure taps, provided a means for a continuous check on flow symmetry.

A T shaped slot, cut into the upper plate, provided access to various radial locations. Various types of probes were mounted on a traversing mechanism consisting of a slide (matched with the slot in the upper plate), and a feed micrometer connected to the probe holders. Several other matching slides, accurately machined, were then used to cover the slot when the measurement probes were put in place. When all slides were in place, the lip between the slides and the upper plate was within ± 0.01 mm.

The uniformity of the flow was checked in several ways: mean velocity measurements at the exit of the settling chamber, static pressure distributions, mean velocity measurement around the outside perimeter of the disks, and by calculating the momentum balance, at various radii and Re, using the mean velocity measurements. The swirl-free state of the flow was verified using a specially designed Pitot static tube. Uniform and symmetric flow was difficult to achieve; even so, the worst indication of non-uniformity was a 5% imbalance between the momentum calculated in the upstream ($r/R_2 = 0.5$) and exit ($r/R_2 = 1.0$) planes at the lowest Reynolds number. This slight difference was believed to be due to the measurement errors at that very small Reynolds number ($Re_m = 18000$, or $Re_{in} \approx 19000$, where $Re_{in} = 2R_1 U_{in}/\nu$).

DISA P12 single-wire boundary-layer probes and DISA P15 slant-wire probes, together with DISA 55M01 CTA bridges were utilized to measure the mean and fluctuating components of the velocity. The error in measuring the mean and r.m.s. velocities caused by the lateral velocity component was calculated from relationships given by Comte-Bellot (1965); as a result, it is estimated that, at the highest intensities measured, the error could be as high as 15%. The error in the slant-wire measurements is higher and this error and its implications will be discussed later.

Pressure measurements were performed using a 0–10 in. (water), Datametric pressure transducer. A floating-element servo-balance mechanism, Nguyen *et al.* (1984), was used for wall-shear-stress measurements at the highest volumetric flow rates; however, this mechanism proved inadequate for measuring the wall shear

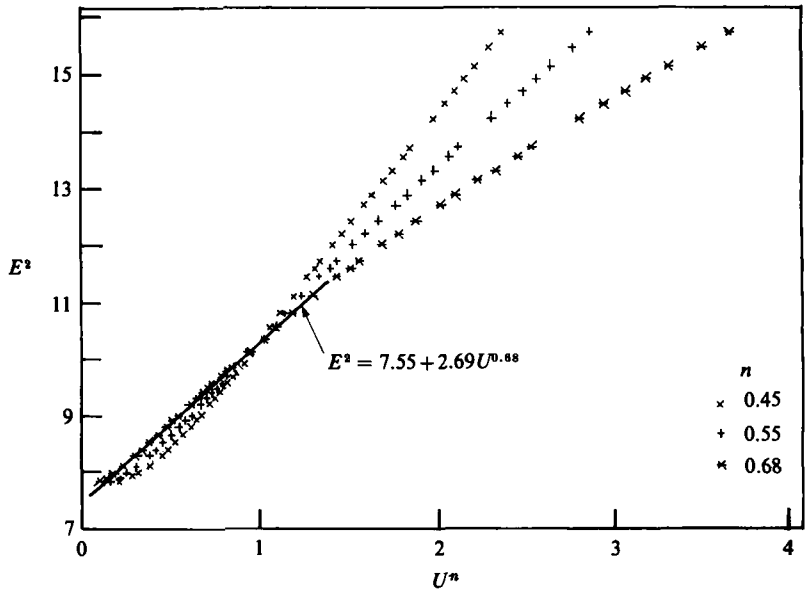

FIGURE 2. The linearized calibration curve.

stress at lower Reynolds numbers. In these cases, estimates of wall shear stress were obtained using the mean velocity gradient in the near-wall region. At high Re, the wall shear stress obtained from the slope of the mean velocity profiles corresponded to within 5% of those obtained using the floating-element device. This discrepancy increased with decreasing Re; and, at the lowest Re, discrepancies of order 30% are possible.

For the present investigation it was necessary to measure very low velocities using hot-wire probes. Calibration of hot-wire probes at low velocities using a conventional jet flow device proved to be both impractical and inaccurate. To calibrate the probes, they were traversed in a stationary fluid at a constant velocity using a self-contained computer-controlled motorized cart (Tabatabai, Pollard & McPhail 1986); it was used in conjunction with the jet flow device. Figure 2 shows a typical linearized calibration curve. Note that in the lower range of the velocities an exponent of 0.68 in King's law provides a more linear representation for the curve. The magnitude of this exponent depends on the velocity range and increases as the velocity becomes smaller.

Hinze's relationship ($U_{\text{eff}} = U^2(\cos^2\alpha + k_\alpha^2 \sin^2\alpha)$) was used to describe the effective velocity felt by the slant wire. The parameter k_α was determined using the procedure of Brunn & Tropea (1980).

The output of the anemometer was corrected for the temperature drift according to Bearman (1971) and also for the effects of conduction in the proximity of the wall, as outlined below.

The location of the hot-wire probe was determined by measuring its distance from its reflection from the aluminium plate through the reticule of a telescope. The error involved in this procedure was estimated to be about 0.01 cm, or about 1% of the gap width.

Data acquisition and reduction was performed using a PDP11/34 minicomputer employing a 12 bit A/D converter. In general about 1024 samples, taken at slow

sampling rates, were used to obtain the moments of the fluctuating signal. The error in the mean and r.m.s. velocity measurements due to sampling size was approximately 4% and 6% respectively, for a confidence level of 97%, using the method suggested by Bates & Hughes (1977). For the determination of the fourth-order moments, Perry (1982) argues that an integration time five times that of the second-order moments is required. Therefore, for the lowest Re, in order to increase the accuracy of the skewness, flatness and probability distributions, 20000 samples (with a sampling rate of 25 Hz) were used. At these same Re, the signal was conditioned (d.c. suppressed and amplified) before passing through the A/D converter.

The spectrum estimates were obtained by block averaging 64 blocks of data, each block generally containing 1024 samples. Sampling rates, varying from 1 to 4 kHz, depending on the flow Re, were used for collecting spectra. The use of 64 blocks decreased the bias in the Fourier transform to below 4%. The major source of error is then the length of the sensing element. This error was found to be as large as 15% at the higher wavenumbers, according to the method proposed by Wyngaard (1968).

3. Presentation and discussion of results

Mean velocity distributions at three Re_{m} are shown in figure 3(a–c). $Re_{l,r}$ in these figures is the Reynolds number based on the gap width $2h$ and local mean velocity U at a given radius r. The asymmetry of the flow displayed in those data in figure 3(a) is a result of the flow negotiating the 90° bend at the inlet. This asymmetry is gradually dissipated by the cross-stream momentum transfer; and the radius at which this asymmetry disappears decreases with the volumetric flow rate. From this figure it can be seen that at high $Re_{l,r}$ the velocity distributions at various radial positions fall within a relatively narrow band. As the volumetric flow rate decreases, the change in the shape of the mean velocity, with increasing radius, becomes more evident: viscous forces begin to dominate those of inertia and the flow tends to a parabolic profile that is reminiscent of laminar channel flow.

Profiles of $U_{\mathrm{mean}}/U_{\mathrm{max}}$ at various Re are shown in figure 4. Note that at very low Reynolds numbers the ratio of mean to maximum velocity goes below a value of 0.66, which would correspond to a parabolic-type distribution. This is due to the inflexion in the near-wall region of the mean velocity profile at low Reynolds numbers; in the literature contradictory evidence for its existence can be found. Higgins (1975) did not mention its existence, although a close examination of his velocity profiles at the smallest Reynolds number does reveal a slight inflexion. Low-Reynolds-number measurements of Bakke & Kreith (1969) and Bakke, Kreider & Krieth (1973), display strong inflexions, which are believed to be augmented by the existence of large wall-proximity errors. The wall-proximity correction procedures available in the literature have been obtained for fully developed turbulent wall flows; see, Azad & Kassab (1986) and the references therein. These corrections were deemed not suitable for the present transition-type flow. Instead, the wall-proximity error was deduced by first creating a two-dimensional channel flow between the disks of the present apparatus. These data displayed no points of inflexion when corrected using a modified form of the Van der Hegge Zijnen corrections (see, for example, Vagt 1979). The radial-flow raw data were subsequently corrected in an analogous manner. In this way, the influence of turbulence generated at the inlet bend, and other possible extrinsic influences, could be accounted for, even at low Reynolds

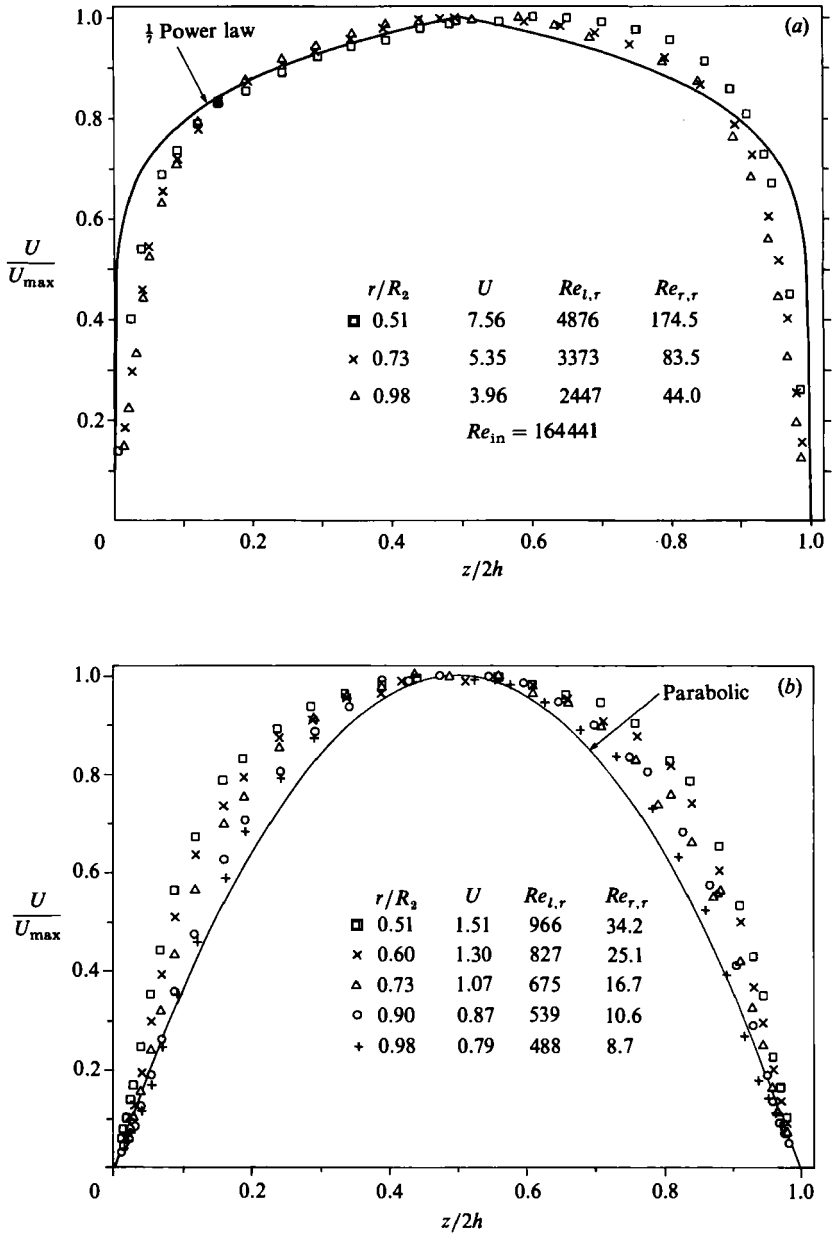

FIGURE 3(*a*,*b*). For caption see facing page.

numbers. Even so, the present results display inflexion points. This topic will be returned to later.

Also shown in figure 4 is the typical variation of mean to maximum velocity for a plane two-dimensional flow deduced from Patel & Head (1969), where it can be seen that for the case of channel flow the transition region is confined to a relatively narrow range of *Re*, while that for the present situation is much broader. Clearly laminar-to-turbulent transition is a more catastrophic event than turbulent-to-laminar transition.

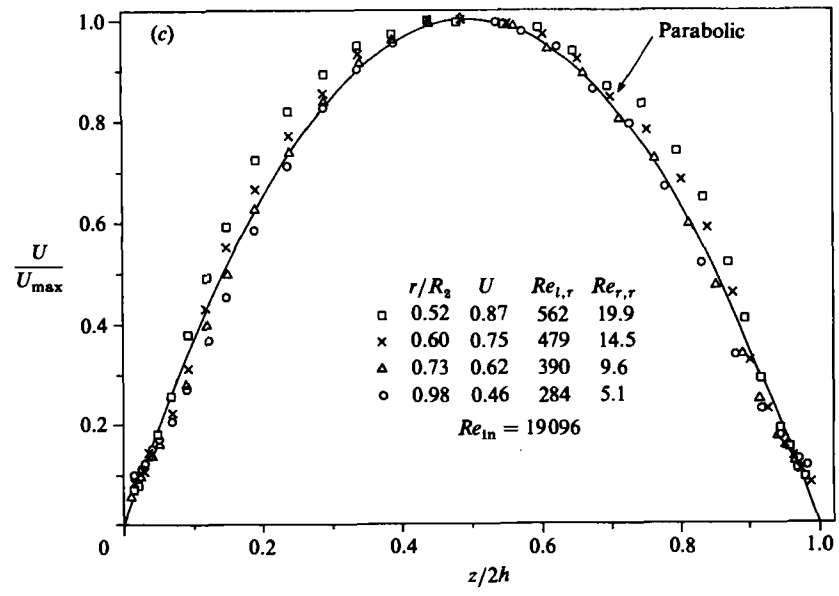

FIGURE 3. Mean velocity distribution across the gap at various radial locations: (*a*) $Re_m = 155000$; (*b*) 31000; (*c*) 18000.

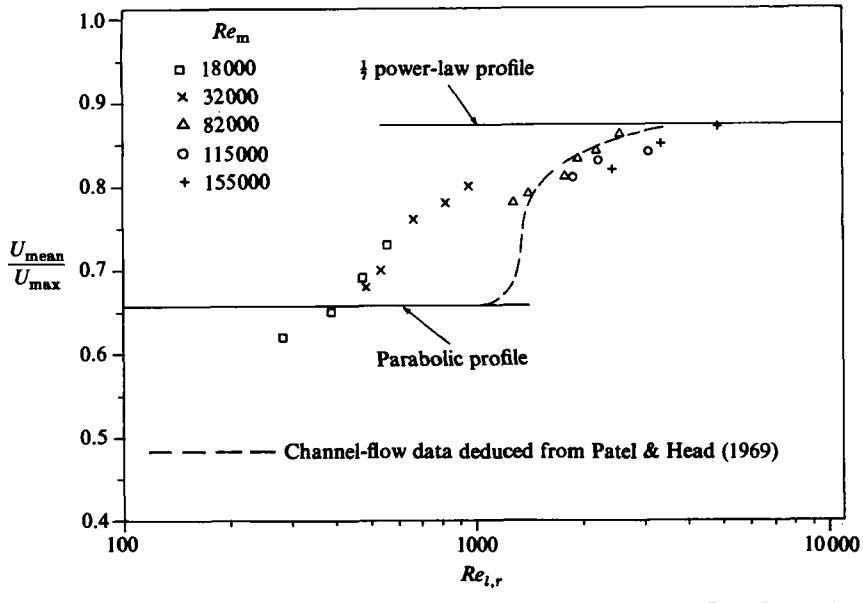

FIGURE 4. Variation of the ratio of the mean to maximum velocity *vs.* $Re_{l,r}$ for various Re_m.

Figure 5 shows the variation of Re_τ, based on the friction velocity and the gap width, versus $Re_{l,r}$. The near-wall velocity gradients were used to estimate the wall shear stresses. Note, however, that at $Re = 155000$, the wall shear stress was obtained using the floating-element device; it is evident that data from this device are in reasonable accord with those obtained using the near-wall velocity-gradient method. The present data are seen to be in agreement with those data from channel flows.

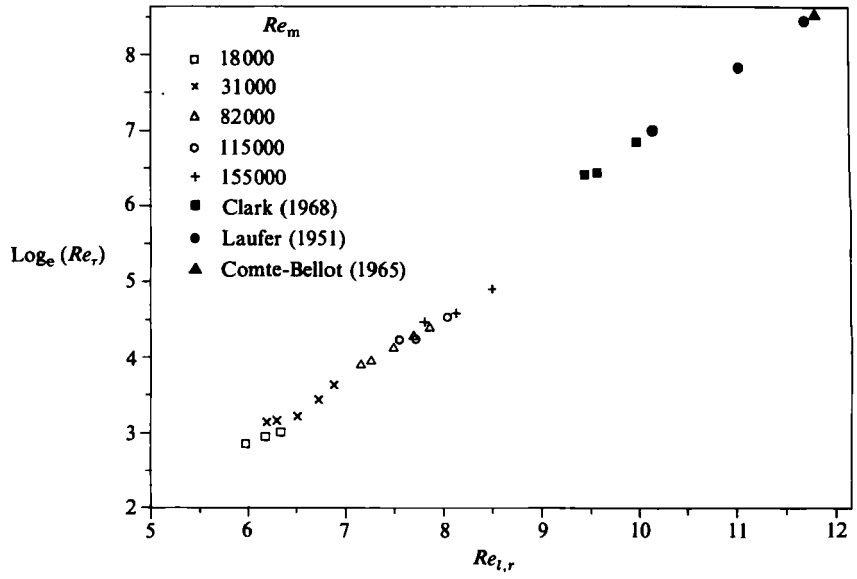

FIGURE 5. Variation of the Reynolds number based on the friction velocity *vs.* $Re_{l,r}$ for various Re_m.

The skin friction in radial flow is defined by the relation $\mathrm{d}P/\mathrm{d}r = \frac{1}{2}\rho\, U^2(C_f/2h)$ and can be written in terms of the wall properties of the flow as $\frac{1}{2}C_f = (U_\tau/U)^2$. Figure 6 shows the variation of the skin friction at various $Re_{l,r}$. At higher Reynolds numbers, the skin-friction curve is compared with $C_f = 0.0376Re^{-\frac{1}{4}}$, which is the relationship obtained in channel flows, Patel & Head (1969). The value of the skin friction increases rapidly at lower Reynolds numbers and displays a transition-type behaviour between $600 < Re_{l,r} < 1000$. The uncertainty in the measurements at the lowest Re prevents any comparison with known laminar-type skin-friction relationships (e.g. $C_f = 12/Re_{l,r}$ as the equivalent for two-dimensional channel flow) or categorically relating the different slopes observed at the smaller Re to the behaviour of the flow.

Figure 7 (*a*, *b*) shows the mean velocities, normalized with the friction velocity, at two Re_m. For comparison, the theoretical velocity distributions in the viscous sublayer:

$$u^+ = z^+, \tag{2}$$

and the logarithmic distribution:

$$u^+ = A\log_{10} z^+ + B, \tag{3}$$

are provided on the figure. The values of A and B are taken as their standard, zero-pressure-gradient values ($A = 5.5$ and $B = 5.45$) even though it has long been recognized that a non-zero pressure gradient can affect the magnitude of these constants; see, for example, McDonald (1969) or Pfeil & Sticksel (1982).

Turbulence intensities, normalized with the maximum velocity across the gap, are shown in figure 8 (*a–c*). At higher Reynolds numbers the maximum value of the intensities are in agreement with those found in two-dimensional channel flows (Clark 1968). At lower Reynolds numbers, and as the flow moves downstream, the location of the point of maximum intensity moves away from the wall; moreover, with increasing radius, its magnitude decreases. Figures 9 and 10 show these

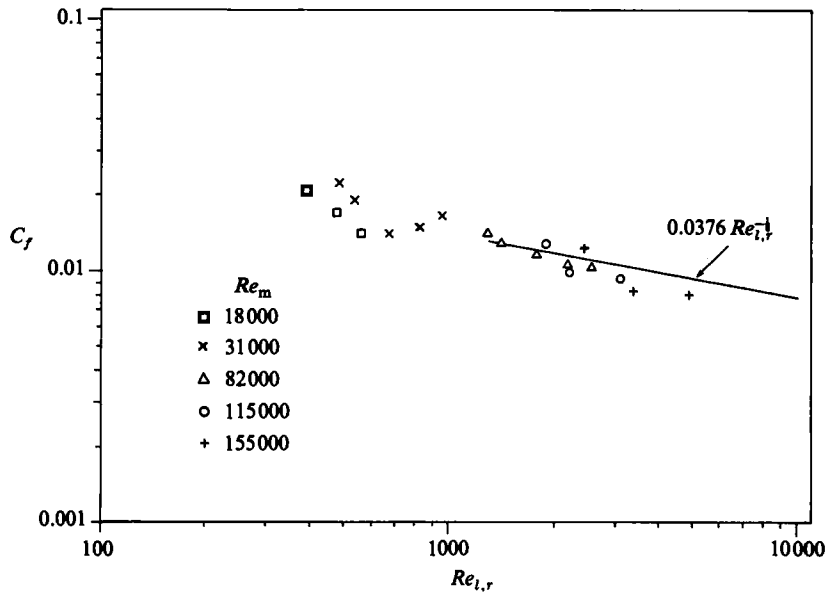

FIGURE 6. Variation of the skin friction *vs.* $Re_{l,r}$ for various Re_m.

variations more clearly. This behaviour indicates a gradual increase in the size of the viscosity-dominated region and a decrease in the rate of energy production in the viscous sublayer with increase in radius. Note that at $Re_m = 18000$ and at the last measuring station (figure 8*c*), the intensity distribution indicates that the maximum value is located on the gap centreline. This behaviour has been attributed to the thickening of the viscous sublayer (Moller 1963; Bakke & Kreith 1969); however, this argument cannot be strictly correct. The velocity distribution in the viscous sublayer is expressed as being proportional to the distance from the wall and is a linear curve. A linear growth of the viscous sublayer would therefore result in a discontinuous velocity distribution across the gap. It is observed that as Re drops, the velocity profile increasingly resembles a laminar-type profile; thus, it is more plausible to assume that during the decay process there occurs a transformation of the viscous sublayer to a laminar-type (or quasi-laminar) boundary layer. The distributions of the intensities normalized with the wall shear stress and probability densities for the low-Re cases, and for other comparisons to be presented shortly, tend to support the latter statement.

From figure 10 it can be seen that the rate of decay of the intensities, even for individual Re_m, is not constant. This behaviour differs from that observed in two-dimensional channel flows where a logarithmic drop in the intensities has been observed (Badri Narayanan 1968).

Figure 11 shows the distribution of the r.m.s. values of the velocity fluctuations, normalized with the friction velocity, against z^+. At higher Re, the value of the maximum normalized intensities (≈ 2.8) and their location ($z \approx 13$) are in good agreement with the channel flow data of Clark (1968). These plots illustrate again the drop in magnitude of the intensities with Reynolds number and radius. In addition, they show clearly that the location of the point of maximum intensity is always at about the same position, irrespective of the radial location and Reynolds number. This tends to support the argument for the existence of a quasi-laminar boundary

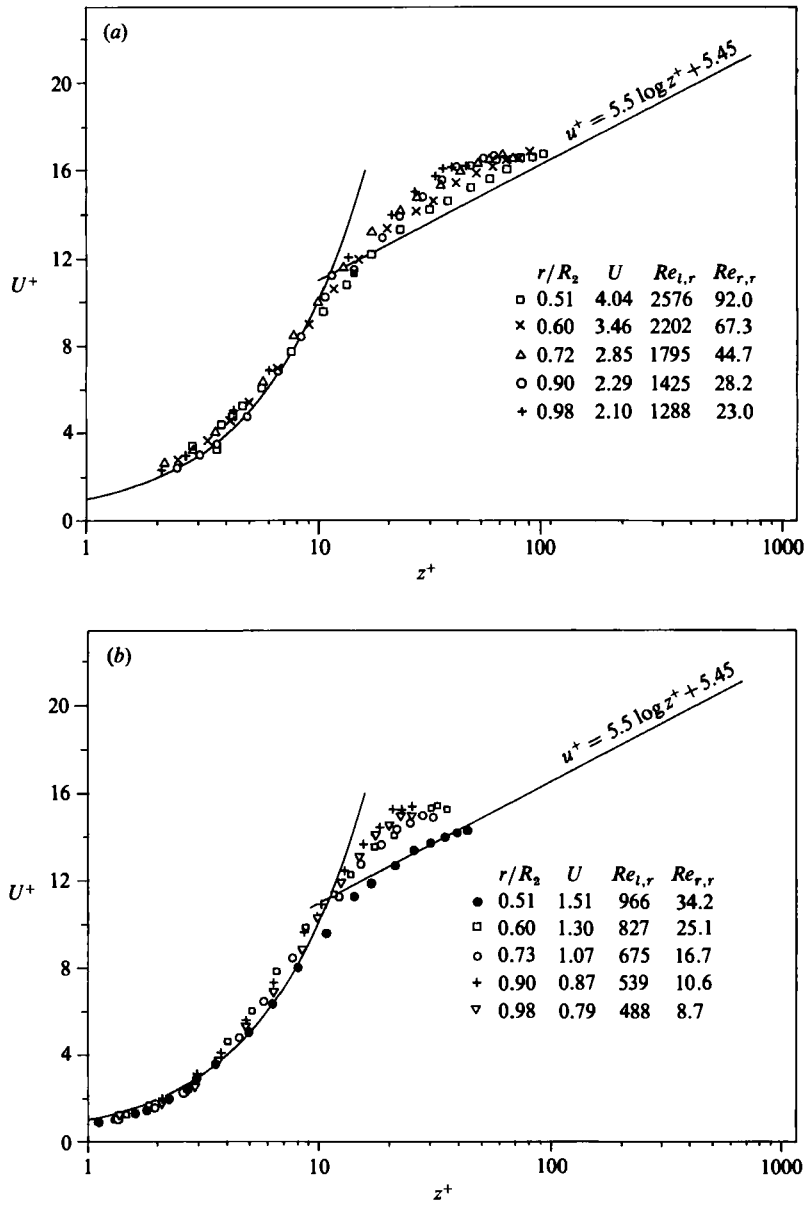

FIGURE 7. Mean velocity distributions, normalized with the wall shear stresses, across the lower half-gap; (*a*) $Re_m = 82000$; (*b*) 31000.

layer and implies the presence of a turbulence mechanism which occurs at low Reynolds numbers, but with similarities to that found at higher Reynolds numbers.

The production of turbulence, according to Reynolds formulation, is the result of work done by the turbulence shear stress against the mean velocity gradient. The present shear-stress measurements, although approximate owing to the relatively large size of the probe sensor compared to the gap width, are, to the authors' knowledge, the first such measurements in this type of flow. Estimates of turbulence shear stresses, normalized with the square of the maximum mean velocity across the

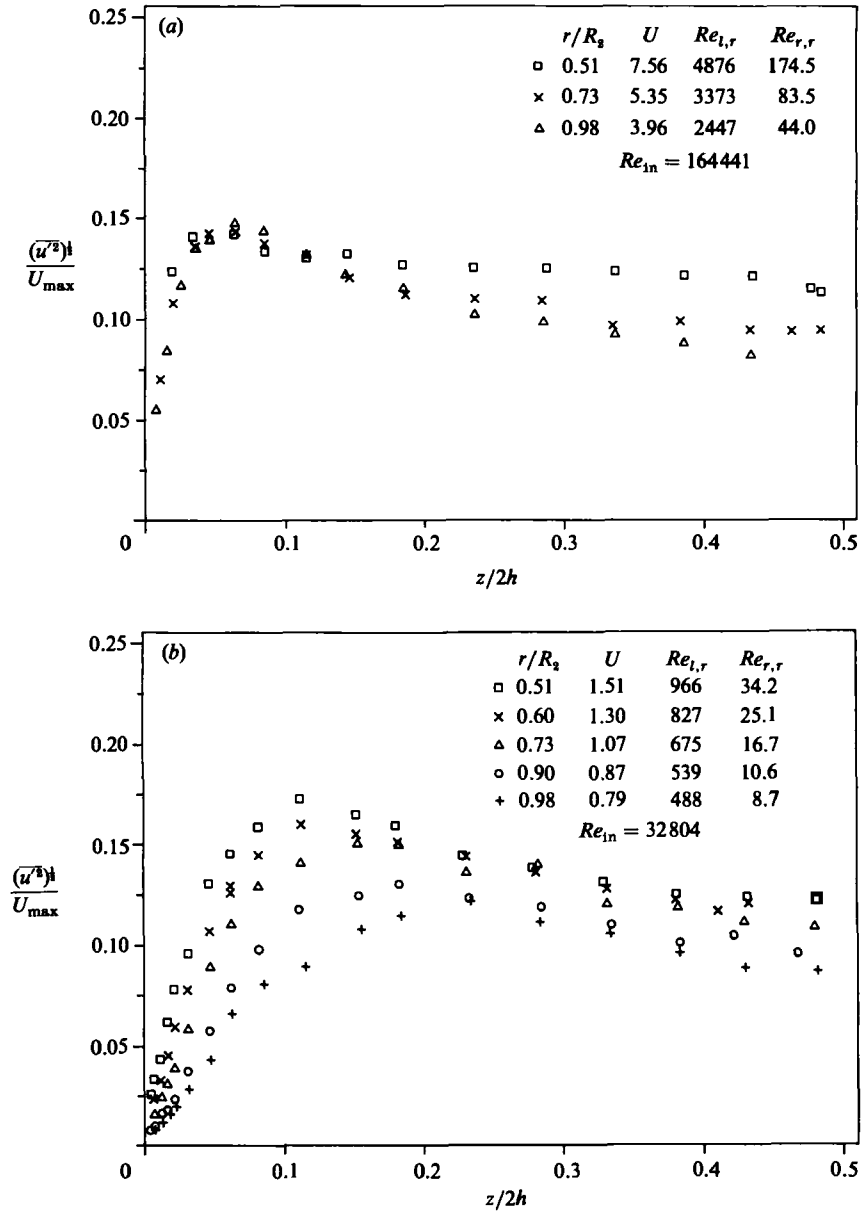

FIGURE 8(*a*,*b*). For caption see page 494.

gap, are presented in figure 12(*a*,*b*). These data are not error free: a consequence of a velocity gradient across the sensor, which results in an underestimation of the shear stresses, particularly in the wall region. The absolute value of the error can be as high as 40% (at the point closest to the wall); however, as the change in the shape of the mean velocity profiles between different radii is small, it is believed that these data can be used for a qualitative assessment of the decay of the shear stresses. From figure 12 it can be seen that at large $Re_{l,r}$ the point of maximum shear stress is located close to the wall where measurements were not possible. As the Reynolds number drops below the transition Reynolds number (corresponding to that of two-

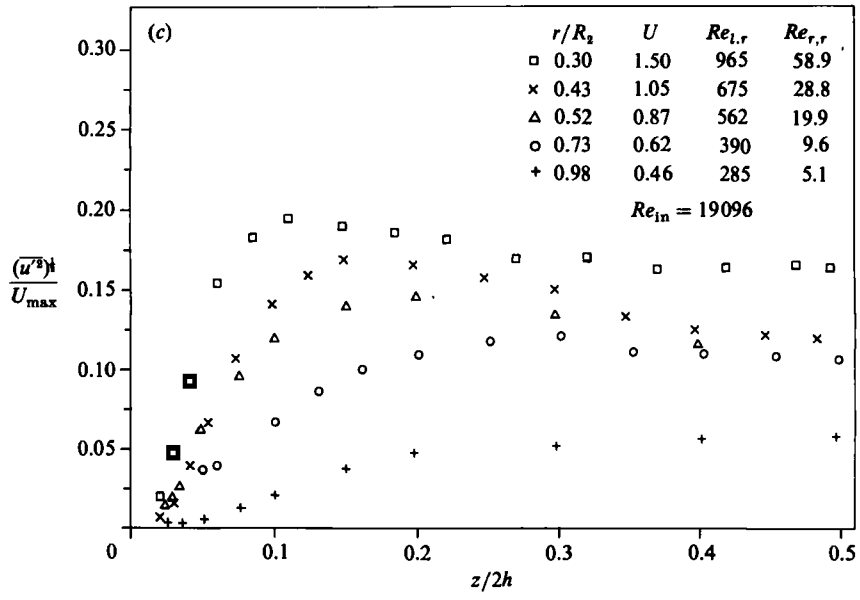

FIGURE 8. Turbulence intensity distributions across the lower half-gap at various radii at (*a*) $Re_m = 155000$, (*b*) 31000, (*c*) 18000.

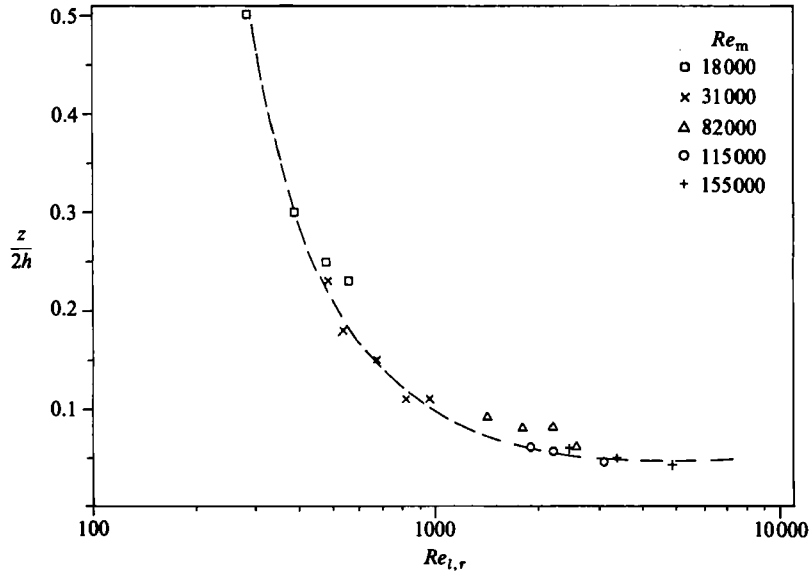

FIGURE 9. Variation of the point of maximum turbulence intensity with $Re_{l,r}$ for various Re_m.

dimensional channel flow, Patel & Head 1969) this point moves away from the wall, all the while decreasing in magnitude.

The distributions of the energy production rate across the gap have been estimated and are presented in figure 13(*a*, *b*). Note the presence of a small but distinct energy production even at the smallest $Re_{l,r}$. Also note the good agreement between the

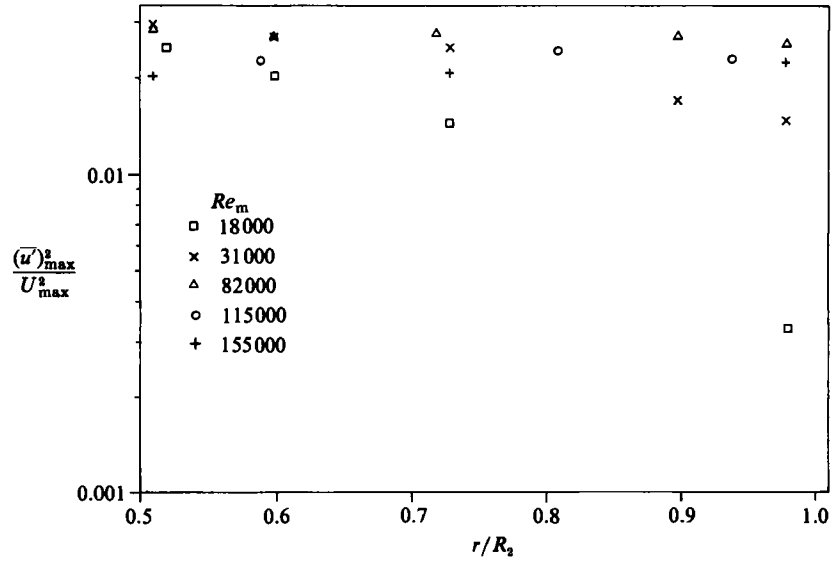

FIGURE 10. Variation of the intensity with radius for various Re_m.

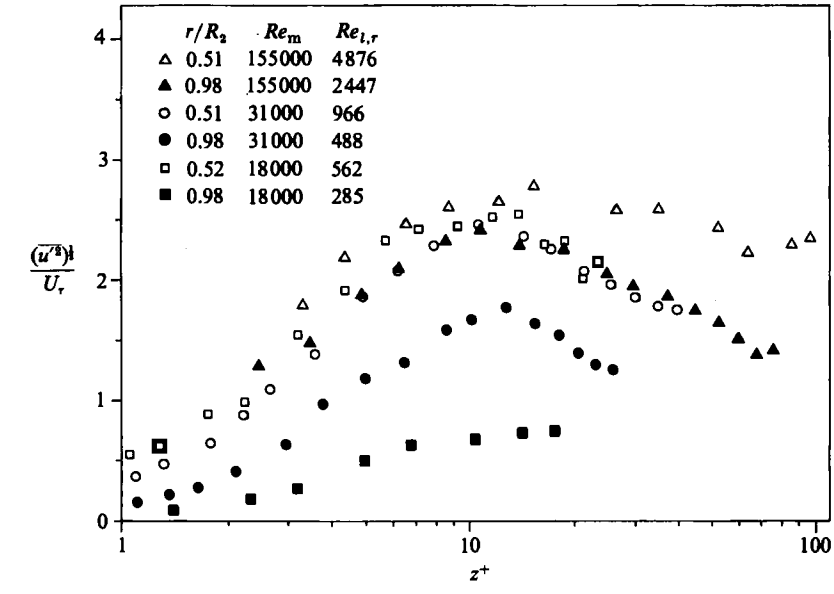

FIGURE 11. Distributions of the intensity, normalized with the friction velocity in the lower half-gap, $Re_m = 155000$.

location of the point of maximum production in figure 13(*b*) and the point of maximum intensity at a similar $Re_{l,r}$ from figure 9.

Probability density distributions were obtained, and those distributions for $Re = 18000$ are shown in figure 14. In general, the probability distributions display behaviour typical of turbulent two-dimensional channel flow (Eckelmann 1974), i.e. large positive skewness close to the wall, a small negative skewness as the distance from the wall increases and a gradual approach to zero skewness as the centreline is

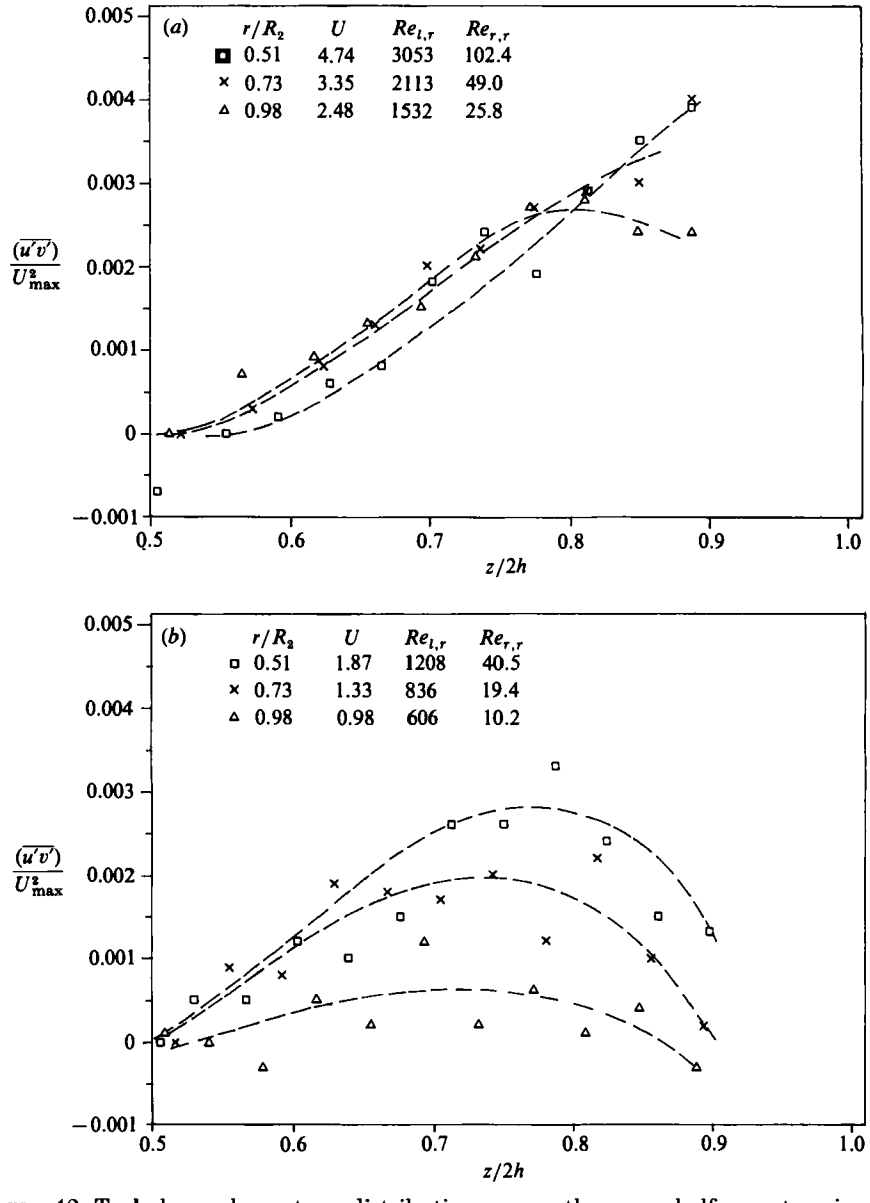

FIGURE 12. Turbulence shear-stress distributions across the upper half-gap at various radii: (*a*) $Re_m = 91000$; (*b*) 36000.

approached. This type of behaviour is clearly observed in figure 14(*a*) (corresponding to $Re_{l,r} = 560$) and it persists, although much more weakly, in the downstream direction at the same Re_m (corresponding to $Re_{l,r} = 285$, figure 14*b*). The implications of these distributions will be discussed below.

The spectral distributions on the centreline at radial locations $r/R_2 = 0.5$ and 0.98, normalized with Λ, are plotted in figure 15 for various Re. Λ is an integral scale obtained from

$$\frac{4\Lambda}{U} = \lim_{n \to 0} \left\{ \frac{1}{\overline{u'^2}} E(n) \right\}, \tag{4}$$

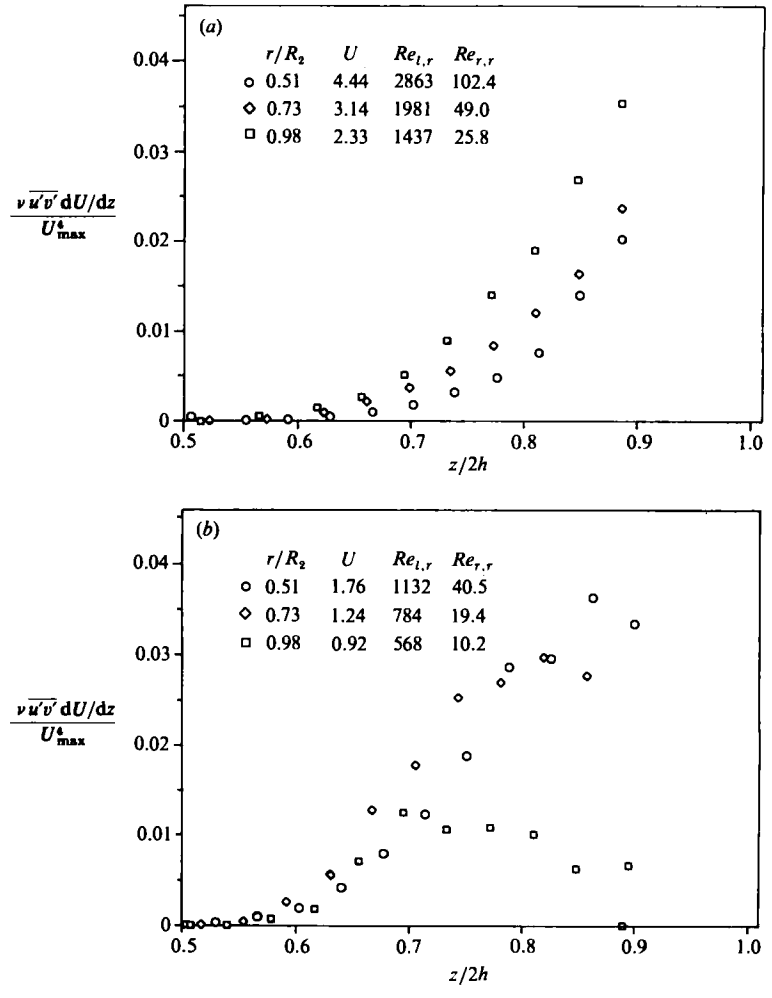

FIGURE 13. Distributions of the turbulent energy-production rate across the upper half-gap: (*a*) $Re_m = 91000$; (*b*) 36000.

where $E(n)$ is the frequency spectrum and n is the frequency. Note the excellent similarity in the spectral distributions obtained at $Re_m = 155000$ and to some extent at $Re_m = 31000$. Previous studies on the turbulence decay in pipe and channel flows (Laufer 1962 and Badri Narayanan 1968, respectively) have produced similar distributions. The latter investigator suggested that the similarity in the spectrum data would result from presuming a local equilibrium in the flow. Figure 15 also shows that similarity no longer exists as Re decreases; and, as the flow moves downstream, the energy at the higher wavenumbers decreases, indicating that the production of turbulence is becoming dominated by dissipation. Hinze (1975) obtained the following relationship, between the spectrum at time t, for the case of isotropic turbulence assuming the interaction among eddies of various sizes is small:

$$E(k,t) = E(k,t_0)\exp\{-2\nu k(t-t_0)\}, \tag{5}$$

where t_0 is some reference time. Based on this equation the decrease in the kinetic energy occurs at a higher rate for smaller eddies compared with the decay rate for

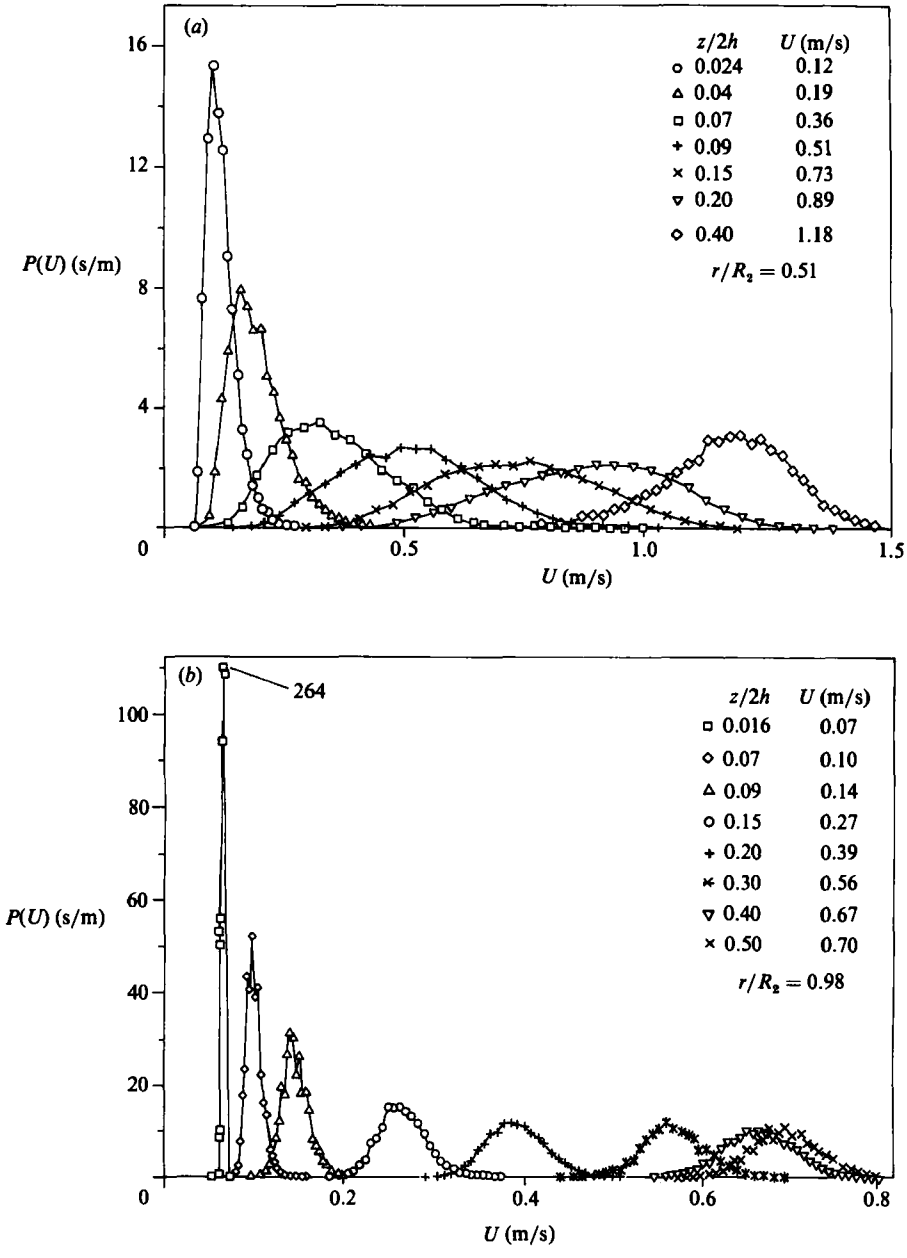

FIGURE 14 (*a*, *b*). Probability density distributions at $Re_m = 18000$; sample size 20000.

larger eddies. Utilizing Taylor's hypothesis for relating time to length, the same type of behaviour can be observed from the present results. In all cases examined, the low-wavenumber energy shows a relatively smaller decrease as the flow moves downstream. Therefore, even at low *Re*, where the production of turbulence was found to be very small, there is, clearly, a persistent large-scale structure.

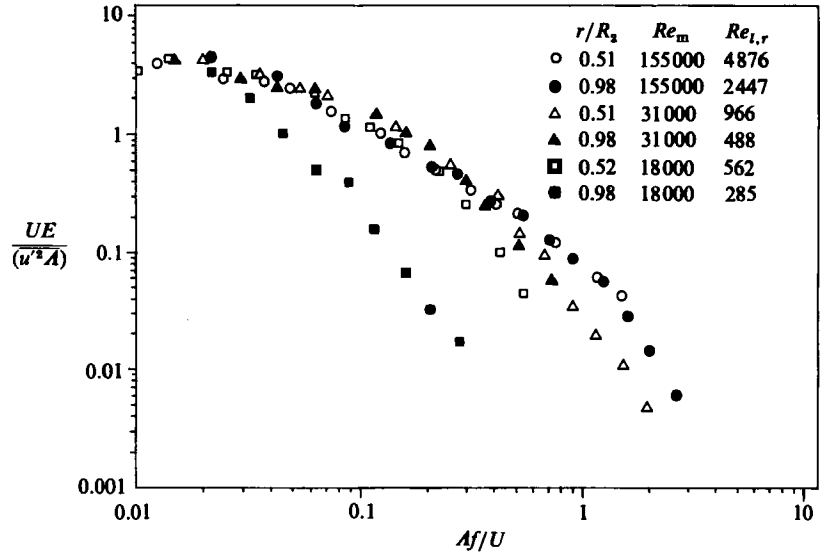

FIGURE 15. Frequency density spectrum distributions normalized with lengthscale Λ, along the gap centreline.

4. Further discussion

Here, use will be made of the wealth of information provided by previous work on two-dimensional channel flows. While this can provide insight into the behaviour of the present flow, the differences between a two-dimensional channel flow and a radial flow should be remembered. Note also that the concept of a fully developed flow does not strictly hold for radial diffusers; furthermore, the geometrical limitation of the apparatus does not permit measurements at $r/2h$ of greater than 60.

Flow-visualization studies in wall-bounded turbulent flows (Kline *et al.* 1967; Kim, Kline & Reynolds 1971, among others) have shown the occurrence of a 'bursting' process in the wall region. This process is often connected to vortices in the near-wall region, particularly to 'hairpin'-types; see, for example Zaric (1982). The bursting process consists of three main phases: ejection of low-momentum flow from the wall vicinity; the breakup of the ejected flow at some distance from the wall corresponding to the edge of the viscous sublayer; and the inrush of the high-momentum fluid towards the wall. A positive value of the skewness factor, close to the wall, is believed to be the consequence of the inrush phase while a negative skewness further from the wall could reflect the ejection process (Zaric 1975). Radial flow at high Reynolds numbers exhibits characteristics very similar to channel flows. Mean velocity, intensity and spectrum profiles correspond closely to fully turbulent two-dimensional channel flows and the probability distributions display indications of the inrush and ejection phases. Although it has yet to be established in the present flow situation, let it be assumed that the bursting-process exists in the flow.

As the flow Reynolds number decreases, the viscous forces begin to dominate the flow as evidenced by the gradual change in the shape of the mean velocity profiles from a $\frac{1}{7}$ power-law type to one that is parabolic in shape, and by the increase in the physical size of the laminar-like near-wall region as indicated by the movement of the point of maximum intensity away from the wall. Assuming that the point of zero skewness and maximum intensity correspond to the breakup location of the ejected

flow, it can be concluded that the breakup occurs further away from the wall; and, since the flow Re decreases as the radius increases, the breakup occurs under weaker inertial forces. Thus, there is a decrease with Re in the rate at which turbulence energy is produced (see figure 13). Although the skin-friction distribution shows a transition region (turbulent-to-laminar) at $Re_{t,r} \approx 600$, some turbulence characteristics, such as a skewed probability distribution, turbulence-intensity distribution with a maximum at $z^+ \approx 13$ and a small energy production rate are observed even at smaller Reynolds numbers. It is hypothesized that the persistent large-scale structure is responsible for this behaviour by delaying the formation of a truly laminar boundary layer; that is, these disturbances provide the necessary element for the continued existence of the ejection phase of the bursting process.

At higher Re, the transport of low-momentum fluid to higher-velocity regions further away from the wall produces a large contribution to the turbulent shear stress and initiates the breakdown of the vortices at their tips. At low Re, however, the vortices must elongate much further to reach the point where this breakdown can occur. Note that the ejection process at higher Re produces a local velocity deficit which is eventually balanced in the inrush phase of the bursting cycle (Zaric 1975). In the present situation, the inflexion in the mean velocity profile observed in figure 3(*c*) can in fact be a consequence of an inrush phase: fluid that is removed during the ejection phase is not totally replaced by that during the inrush phase; however, note that mass is conserved at any given radius. As Re drops even further, it is likely that, although the ejection phase occurs, nowhere across the gap does the tip of a hairpin vortex come under strong enough shear to breakdown. Indeed, as the tip approaches the centreline, as it must do as Re approaches zero, the possibility of breakdown is completely eliminated since the velocity gradient there is zero.

The spectrum results of figure 15 show that at $Re_m = 18000$, somewhere between $0.5 < r/R_2 < 0.98$ the turbulence production is completely halted. The flow, after passing through this region, will still contain residuals of turbulence produced upstream in the high-Re portion of the flow which have to be dissipated before a truly laminar state can be reached. The results of the measurements at the lowest Re of figure 14(*b*), when compared to the corresponding upstream measurement of figure 14(*a*) indicate the approach to this state. Relaminarization is therefore believed to occur, not as a catastrophic process occurring at a given critical radius, but as a very slow turbulence decay process.

5. Conclusion

A comprehensive study of the radial flow between parallel disks at medium and low Reynolds numbers was carried out. At higher Reynolds numbers the flow displays characteristics very similar to those of fully developed channel flows. At these Reynolds numbers, the inertial forces are large enough that, at different radial locations, no significant change in the flow behaviour was observed, except that corresponding to the development of the flow. As the Reynolds number decreases, however, the thickness of the viscosity-dominated region increases, at a rate approximately proportional to the inverse of the local Reynolds number. It was suggested that during this growth process, the viscous sublayer is transformed into a quasi-laminar boundary layer. The turbulence state decays, but this decay, unlike that observed in a channel flow, is not logarithmic along the whole radius and was found to be more complex (in the present range of r/h at least two logarithmic rates of decay can be observed at low volumetric flow rates). The spectrum results

displayed a local equilibrium at high and medium *Re*, which is eventually destroyed as the thickness of the quasi-laminar boundary layer increases towards the gap centreline. The spectrum distributions also indicate the persistence of a large-scale structure throughout the flow, which is believed to be the mechanism that maintains the turbulence characteristics of the quasi-laminar sublayer. Relaminarization is the final outcome of the decay mechanism.

Financial assistance was provided by the Natural Science and Engineering Research Council of Canada and Queen's University, School of Graduate Studies. The authors acknowledge with thanks the donation of the aluminium plates by the Aluminium Company of Canada (ALCAN), Kingston, Ontario.

REFERENCES

AZAD, R. S. & KASSAB, S. Z. 1986 Measurements of small distance in proximity of a wall with a hot wire. *Presented at AIAA/ASME Joint Fluid Mechanics, Plasma Dynamics and Lasers Conference, Atlanta, Georgia, May.*

BADRI NARAYANAN, M. A. 1968 An experimental study of reverse transition in two-dimensional channel flow. *J. Fluid Mech.* **31**, 609.

BAKKE, E., KREIDER, J. F. & KREITH, F. 1973 Turbulent source flow between parallel stationary and co-rotating disks. *J. Fluid Mech.* **58**, 209.

BAKKE, E. & KREITH, F. 1969 Inverse transition in radial diffusers. *ASME-AIChE Heat Transfer Conference, Minneapolis, Minn., Paper* 69-HT-33.

BATES, C. J. & HUGHES, T. D. R. 1977 The effect of both sampling size and sampling rate on the statistical fluid flow parameters in high Reynolds number low turbulence intensity flows. *Proc. 5th Symposium on Turbulence, University of Missouri–Rolla.*

BEARMAN, P. W. 1971 Corrections for the effect of ambient temperature drift on hot-wire measurements in incompressible flow. *DISA Information*, 11, p. 25.

BRUNN, H. H. & TROPEA, C. 1980 Calibration of normal, inclined and X-array hot wire probes. *Rep.* SFB 80/M/170, University of Karlsruhe. See also, *J. Phys.* E: *Sci. Instrum.* **18**, 405.

CHEN, C. P. & PEUBE, J. L. 1966 *C. R. Acad. Sci. Paris* **250**, 5353.

CLARK, J. A. 1968 A study of incompressible turbulent boundary layers in channel flow. *Trans. ASME* D: *J. Basic Engng* **90**, 455.

COMTE-BELLOT, G. 1965 Ecoulement turbulent entre deux parious paralleles. *Publication Sci. et Tech. du Ministere de L'Air* 419.

ECKELMANN, H. 1974 The structure of the viscous sublayer and the adjacent wall region in a turbulent channel flow. *J. Fluid Mech.* **65**, 439.

HIGGINS, G. B. 1975 Some aspects of radial flow between parallel disks. M.Sc. thesis, University of Witwatersrand, S. Africa.

HINZE, J. O. 1975 *Turbulence*, 2nd edn. McGraw Hill.

ISHIZAWA, S. 1965 The axisymmetric laminar flow in an arbitrarily shaped narrow gap, 1st Report. *Bull. JSME* **8**, 353.

ISHIZAWA, S. 1966 The axisymmetric laminar flow in an arbitrarily shaped narrow gap, 2nd Report. *Bull. JSME* **9**, 86.

JACKSON, J. D. & SYMMONS, G. R. 1965 The pressure distribution in a hydrostatic thrust bearing. *Intl J. Mech. Sci.* **7**, 239.

KIM, H. T., KLINE, S. J. & REYNOLDS, W. C. 1971 The production of turbulence near a smooth wall in a turbulent boundary layer. *J. Fluid Mech.* **50**, 133.

KLINE, S. J., REYNOLDS, W. C., SCHRAUB, F. A. & RUNSTADLER, P. W. 1967 The structure of turbulent boundary layers. *J. Fluid Mech.* **30**, 741.

KREITH, F. 1966 Reverse transition in radial source flow between two parallel planes. *Phys. Fluids* **8**, 1189.

LAUFER, J. 1962 Decay of a non-isotropic turbulent field. In *Mitteilungen der Angewandten Mechanik* (ed. M. Schaefer), p. 166. Göttingen.

LIVESEY, J. L. 1959 Inertia effects in viscous flow. *Intl J. Mech. Sci.* **1**, 84.

MCDONALD, H. 1969 The effect of pressure gradient on the law of the wall in turbulent flow. *J. Fluid Mech.* **35**, 311.

MCGINN, J. H. 1955 Radial flow between parallel plates. *Appl. Sci. Res.* **5**, 255.

MOCHIZUKI, S. & YANG, W. 1983 Flow separation and heat transfer in radial flows between two parallel disks. *Bull. JSME* **49**, 48.

MOCHIZUKI, S. & YANG, W. 1985 Self-sustained radial oscillating flows between parallel disks. *J. Fluid Mech.* **154**, 377.

MOCHIZUKI, S., YANG, W. & TANAKA, M. 1986 Flow visualisation in radial flow through stationary and rotating parallel disks. *Proc. 4th Intl Symp. on Flow Visualisation, Paris* (ed. C. Véret), pp. 297–302. Hemisphere.

MOLLER, P. S. 1963 Radial flow without swirl between parallel disks. *Aero. Q.* **14**, 163.

MOLLER, P. S. 1966 A radial diffuser using incompressible flow between narrowly spaced disks. *Trans. ASME* D: *J. Basic Engng* **88**, 155.

NGUYEN, V. D., DICKINSON, J., JEAN, Y., CHALIFOUR, Y., ANDERSON, J., LENCAY, J., HAEBERLE, D. & LAROSE, G. 1984 Some experimental observations of the law of the wall behind large-eddy break-up devices using servo-controlled skin friction balances. *22nd AIAA Aerospace Science Meeting, Reno, Nevada, Paper* 84-0346.

PATEL, V. C. & HEAD, M. R. 1969 Some observations on skin friction and velocity profiles in fully developed pipe and channel flows. *J. Fluid Mech.* **38**, 187.

PERRY, A. E. 1982 *Hot Wire Anemometry*. Oxford University Press.

PFEIL, H. & STICKSEL, W. J. 1982 Influence of the pressure gradient on the law of the wall. *AIAA J.* **20**, 434.

SAVAGE, S. B. 1964 Laminar radial flow between parallel disks. *Trans. ASME*, **31**, 594.

TABATABAI, M. 1985 Transport processes in two dimensional radial flow between parallel disks. Ph.D. thesis, Queen's University at Kingston, Ontario, Canada.

TABATABAI, M., POLLARD, A. & MCPHAIL, A. 1986 A device for calibrating hot-wire probes at low velocities. *J. Phys.* E: *Sci. Instrum.* **19**, 630.

VAGT, J. D. 1979 Hot wire probes in low speed flow. *Prog. Aerospace Sci.* **18**, 271.

WYNGAARD, J. C. 1968 Measurement of small scale turbulence structure with hot wires. *J. Phys.* E: *Sci. Instrum.* **1**, 1105.

ZARIC, Z. 1975 Wall turbulence structure and convection heat transfer. *Intl J. Heat Mass Transfer* **18**, 831.

ZARIC, Z. (ed.) 1982 Structure of turbulence in heat and mass transfer. *Proc. ICHMT Symp. on Heat and Mass Transfer and the Structure of Turbulence.* Hemisphere.